

# Hierarchical space-time modeling of exceedances with an application to rainfall data

Jean-Noel Bacry<sup>†</sup>, Carlo Gaetan<sup>‡</sup>, Thomas Opitz<sup>¶</sup>, Gwladys Toulemonde<sup>†</sup>

<sup>†</sup>IMAG, Université de Montpellier, Montpellier, France

<sup>‡</sup>DAIS, Università Ca' Foscari di Venezia, Venice, Italy

<sup>¶</sup>BioSP, INRA, Avignon, France

April 28, 2022

## Abstract

The statistical modeling of space-time extremes in environmental applications is key to understanding complex dependence structures in original event data and to realistic scenario generation for impact models. In this context of high-dimensional data, we propose a novel hierarchical model for high threshold exceedances defined over continuous space and time by embedding a space-time Gamma process convolution for the rate of an exponential variable, leading to asymptotic independence in space and time. Its physically motivated anisotropic dependence structure is based on geometric objects moving through space-time according to a velocity vector. We demonstrate that inference based on weighted pairwise likelihood is efficient both statistically and computationally. The usefulness of our model is illustrated by an application to hourly precipitation data from a study region in Southern France, where it clearly improves on an alternative censored Gaussian space-time random field model. While classical limit models based on max-stability fail to appropriately capture relatively fast joint tail decay rates between asymptotic dependence and classical independence, strong empirical evidence

from our application and other recent case studies motivates the use of more realistic asymptotic independence models such as ours.

*Keywords:* Asymptotic independence, composite likelihood, space-time convolution, gamma random fields, hourly precipitation.

## 1. INTRODUCTION

Fueled by important environmental applications, the statistical modeling of spatial extremes has undergone a fast evolution during the last decade. An important shift from maxima-based modeling to approaches using threshold exceedances can be observed over recent years, whose reasons lie in the capability of thresholding techniques to exploit more information from the data and to explicitly model the original event data. A first overview of typical approaches to modeling maxima is due to Davison et al. (2012). A number of hierarchical models based on latent Gaussian processes (Casson and Coles, 1999; Gaetan and Grigoletto, 2007; Cooley et al., 2007; Sang and Gelfand, 2009) have been proposed, but they may be criticized for relying on the rather rigid Gaussian dependence with very weak dependence in the tail, while the lack of closed-form marginal distributions makes interpretation difficult and non-Bayesian inference cumbersome. Max-stable random fields (Smith, 1990; Schlather, 2002; Kabluchko et al., 2009; Davison and Gholamrezaee, 2012; Opitz, 2013) are the natural limit models for maxima data and have spawned a very rich literature, from which the model of Reich and Shaby (2012) stands out for its hierarchical construction simplifying high-dimensional multivariate calculations and Bayesian inference. Generalized Pareto processes (Ferreira and de Haan, 2014; Thibaud and Opitz, 2015) are the equivalent limit models for threshold exceedances. However, the asymptotic dependence stability in these limiting processes for maxima and threshold exceedances has a tendency to be overly restrictive when asymptotic dependence strength decreases at high levels and may vanish ultimately in the case of asymptotic independence. Such behavior appears to be characteristic for many real data sets such as precipitation (Davison et al., 2013; Thibaud et al., 2013) and has motivated the development of more flexible dependence models such as max-mixtures of max-stable and asymptotically independent processes (Wadsworth and Tawn, 2012; Bacro et al., 2016) for maxima data, and Gaussian scale mixture processes (Opitz, 2016; Huser et al., 2017) for threshold exceedances, capable to accommodate asymptotic dependence, asymptotic independence and Gaussian dependence with a smooth transition. Gaussian scale mixtures can be viewed as part of the wider class of copula models (see Bortot et al., 2000; Davison et al., 2013, for other examples) typically combining univariate limit distributions with dependence structures that should ideally be flexible and relatively easy to handle in practice.

Statistical inference is then often carried out assuming temporal independence in measurements typically observed at spatial sites at regularly spaced time intervals. However, developing flexible space-time modeling for extremes is crucial for characterizing the temporal persistence of extreme events spanning several time steps; such models are important for short-term prediction in applications such as the forecasting of wind power and atmospheric pollution, and for extreme event scenario generators providing inputs to impact models, for instance in hydrology and agriculture. Currently, only few models are available in the statistical literature. Davis and Mikosch (2008) considered extremal properties of heavy-tailed moving average processes where coefficients and the white-noise process depend on space and time, but their work was not focused on practical modeling. Sang and Gelfand (2009) proposed a hierarchical procedure for maxima data but limited to latent Gauss–Markov random fields. Davis et al. (2013a,b) extend the widely used class of Brown–Resnick max-stable processes to the space-time framework and propose pairwise likelihood inference. Spatial max-stable processes with random set elements have been proposed by Schlather (2002); Davison and Gholamrezaee (2012), and Huser and Davison (2014) have fitted a space-time version to threshold exceedances of hourly rainfall data through pairwise censored likelihood. A Bayesian approach based on spatial skew- $t$  random fields with a random set element and temporal autoregression was proposed by Morris et al. (2017). The aforementioned space-time models may capture asymptotic dependence or exact asymptotic independence at small distances but are unsuitable when dealing with residual dependence in asymptotic independence. In this paper, we propose a novel approach to space-time modeling of asymptotically independent data to avoid the tendency of max-stable like models to potentially strongly overestimate joint extreme risks. In a similar context, Nieto-Barajas and Huerta (2017) have recently proposed a spatio-temporal Pareto model for heavy-tail data on spatial lattices, generalizing the temporal latent process model of Bortot and Gaetan (2014) to space-time.

Our model provides a hierarchical formulation for modeling spatio-temporal exceedances over high thresholds. It is defined over a continuous space-time domain and allows for a clear physical interpretation of extreme events spreading over space and time. Strong motivation also comes from Bortot and Gaetan (2014) by developing a generalization of their latent temporal process. Alternatively, our latent process could be viewed as a space-time version of the temporal trawl processes introduced by Barndorff-Nielsen

et al. (2014). Our approach is based on representing a generalized Pareto distribution as a Gamma mixture of an exponential distribution, enabling us to keep easily tractable marginal distributions which are coherent with univariate extreme value theory. Our key idea is to use a kernel convolution of a space-time Gamma random process (Wolpert and Ickstadt, 1998a) based on influence zones defined as cylinders with an ellipsoidal basis to generate anisotropic spatio-temporal dependence in exceedances. We then develop statistical inference based on a pairwise composite likelihood approach.

The paper is structured as follows. Our hierarchical model with a detailed description of its two stages and marginal transformations is developed in Section 2. Space-time Gamma random fields are presented in Section 2.1, where we also propose the construction and formulas for the space-time objects used for kernel convolution. Section 3 characterizes tail dependence behavior in our new model yielding asymptotic independence in space and time. Statistical inference of model parameters is addressed in Section 4 based on a pairwise log-likelihood for the observed censored excesses. We show estimation efficiency through a simulation study presented in Section 5 involving two scenarios of different complexity. In Section 6, the application to hourly precipitation data from a study region in Southern France illustrates the usefulness of our model in practice. Since a natural choice of a reference model for asymptotically independent data is to use a threshold-censored space-time Gaussian process, we show the good relative performance of our model by comparing it to such an alternative. A discussion of our modeling approach with some potential future extensions closes the paper in Section 7.

## 2. A HIERARCHICAL MODEL FOR SPATIO-TEMPORAL EXCEEDANCES

When dealing with exceedances of a random variable  $X$  above a high threshold  $u$ , univariate extreme value theory suggests using the limit distribution of Generalized Pareto (GP) type. The GP cumulative distribution function (cdf) is defined for any  $y > 0$  by

$$GP(y; \sigma, \xi) = 1 - \left(1 + \xi \frac{y}{\sigma}\right)_+^{-(1/\xi)}, \quad (1)$$

where  $(a)_+ = \max(0, a)$ ,  $\xi$  is a shape parameter and  $\sigma$  a positive scale parameter. The sign of  $\xi$  characterizes the maximum domain of attraction of the distribution of  $X$ :  $\xi > 0$  corresponds to the Fréchet domain of

attraction while  $\xi = 0$  and  $\xi > 0$  correspond to the Gumbel and Weibull ones, respectively.

When  $\xi > 0$ , the GP distribution can be expressed as a Gamma mixture for the rate of the exponential distribution (Reiss and Thomas, 2007, p.157), i.e.

$$V|\Lambda \sim \text{Exp}(\Lambda), \quad \Lambda \sim \text{Gamma}(1/\xi, \sigma/\xi) \quad \Rightarrow \quad V \sim GP(\cdot; \sigma, \xi), \quad (2)$$

where  $\text{Exp}(b)$  refers to the Exponential distribution with rate  $b > 0$  and  $\text{Gamma}(a, b)$  to the Gamma distribution with shape  $a > 0$  and rate  $b > 0$ . Based on this hierarchical structure, we will here develop a stationary space-time construction for modeling exceedances over a high threshold, which possess marginal GP distributions for the strictly positive excess above the threshold. Nonstationarities in our model can arise in the marginal distributions.

## 2.1 First stage: generic hierarchical space-time structure

We consider a stationary space-time random field  $Z = \{Z(x), x \in \mathcal{X}\}$  with  $x = (s, t)$  and  $\mathcal{X} = \mathbb{R}^2 \times \mathbb{R}^+$ , such that  $s$  indices spatial location and  $t$  time. Without loss of generality, we assume that the margins  $Z(x)$  belong to the Fréchet domain of attraction with positive shape parameter  $\xi$ . To infer the tail behavior of  $\{Z(x)\}$ , we focus on values exceeding a fixed high threshold  $u$ , and we consider the exceedances over  $u$ ,

$$Y(x) = (Z(x) - u) \cdot \mathbb{1}_{(u, \infty)}(Z(x)). \quad (3)$$

Standard results from extreme value theory (de Haan and Ferreira, 2006) establish the *GP* distribution with  $\xi > 0$  in (1) as the limit of suitably renormalized positive threshold exceedances in (3), such that it represents a natural model for the values  $Y(x) > 0$ . Following Bortot and Gaetan (2014), we use the representation of the *GP* distribution as a Gamma mixture of an exponential distribution to formulate a two-stage model that induces spatio-temporal dependence arising in both the exceedance indicators  $\mathbb{1}_{(u, \infty)}(Z(x))$  and the positive excesses  $Z(x) - u > 0$  by integrating space-time dependence in a latent Gamma component. A key feature of our model is that it naturally links exceedance probability to the size of the excess and therefore provides a joint space-time structure of the zero part and the positive part in the zero-inflated distribution of  $Y(x)$ .

In the first stage, we condition on a latent space-time random field  $\{\Lambda(x)\}$  with marginal distributions  $\Lambda(x) \sim \text{Gamma}(\alpha, \beta)$  and assume that

$$Y(x) \mid [\Lambda(x), Y(x) > 0] \sim \text{Exp}(\Lambda(x)), \quad (4a)$$

$$\Pr(Y(x) > 0 \mid \Lambda(x)) = e^{-\kappa\Lambda(x)}, \quad (4b)$$

where  $\kappa > 0$  is a parameter controlling the rate of upcrossings of the threshold. The resulting marginal distribution of  $Y(x)$  conditionally on  $Z(x) > u$  corresponds to the GP distribution, and the unconditional marginal cdf of  $Y(x)$  is

$$F(y; \sigma, \xi) = \begin{cases} p & \text{for } y = 0, \\ p + (1-p)GP(y; \xi, \sigma) & \text{for } y > 0, \end{cases} \quad (5)$$

with shape parameter  $\xi = 1/\alpha$ , scale parameter  $\sigma = (\kappa + \beta)/\alpha$ , and with  $1 - p$  the probability of an exceedance over  $u$ , i.e.  $\Pr(Z(x) > u) = \Pr(Y(x) > 0) = 1 - p$ . The probability of exceeding  $u$ ,

$$\Pr(Z(x) > u) = \mathbb{E}(\Pr(Y(x) > 0 \mid \Lambda(x))) = \mathbb{E}(e^{-\kappa\Lambda(x)}) = \left(\frac{\beta}{\kappa + \beta}\right)^\alpha \quad (6)$$

depends on  $\kappa$  and it is the Laplace transform of  $\Lambda(x)$  evaluated at  $\kappa$ . The constraint  $\xi > 0$  would be overly restrictive for general modeling purposes, but we can relax it by following Bortot and Gaetan (2016): we consider a marginal transformation within the class of GP distributions for threshold exceedances, for which we suppose that  $\alpha = 1$  and  $\beta = 1$  for identifiability. By transforming  $Y(x)$  through the probability integral transform

$$g(y) = GP^{-1}(GP(y; 1, 1 + \kappa); \sigma^*, \xi^*) = (\sigma^*/\xi^*) \left\{ \left(1 + \frac{y}{\kappa + 1}\right)^{\xi^*} - 1 \right\} \quad (7)$$

with parameters  $\xi^* \in \mathbb{R}$  and  $\sigma^* > 0$  to be estimated, we get a marginally transformed random field  $Y^*(x) = g(Y(x))$  which satisfies  $Y^*(x) \sim GP(\cdot; \xi^*, \sigma^*)$ , conditionally on  $Y^*(x) > 0$ . Notice that it is straightforward to develop extensions with nonstationary marginal excess distributions by injecting response surfaces  $\sigma^*(x)$  and  $\xi^*(x)$  into (7).

## 2.2 Second stage: space-time dependence with Gamma random fields

Spatio-temporal dependence is introduced by means of a space-time stationary random field  $\{\Lambda(x), x \in \mathcal{X}\}$  with  $\text{Gamma}(\alpha, \beta)$  marginal distributions. In principle, we could use an arbitrarily wide range of

models with any kind of space-time dependence structure, for instance by marginally transforming a space-time Gaussian random field using the copula idea (Joe, 1997). However, we here aim to propose a construction where Gamma marginal distributions arise naturally without applying rather artificial marginal transformations. Inspired by the gamma process convolutions of Wolpert and Ickstadt (1998a), we develop a space-time gamma convolution process with gamma marginal distributions. The kernel shape in our construction allows for a straightforward interpretation of the dependence structure, and it offers a 'physical' interpretation of real phenomena such as mass and participle transport. Moreover, we obtain simple analytical formulas for the bivariate distributions, which facilitates statistical inference, interpretation and the characterization of joint tail properties.

We fix  $\mathcal{X} = \mathbb{R}^d$  and consider  $A \in \mathcal{B}_b(\mathcal{X})$ , a subset of  $\mathcal{X}$  belonging to the  $\sigma$ -field  $\mathcal{B}_b(\mathcal{X})$  restricted to bounded sets of  $\mathcal{X}$ . A gamma random field  $\Gamma(dx)$  (Ferguson, 1973) is a non negative random measure defined on  $\mathcal{X}$  characterized by a base measure  $\alpha(dx)$  and an inverse scale parameter  $\beta$  such that

1.  $\Gamma(A) := \int_A \Gamma(dx) \sim \text{Gamma}(\alpha(A), \beta)$ , with  $\alpha(A) := \int_A \alpha(dx)$ ;
2. for any  $A_1, A_2 \in \mathcal{B}_b(\mathcal{X})$  such that  $A_1 \cap A_2 = \emptyset$ ,  $\Gamma(A_1)$  and  $\Gamma(A_2)$  are independent random variables.

The calculation of the principal formulas in this paper relies on the Laplace exponent of the random measure

$$\mathcal{L}(\phi) := -\log \mathbb{E} \left( \exp \left\{ - \int \phi(x) \Gamma(dx) \right\} \right) = \int_{\mathcal{X}} \log \left\{ 1 + \frac{\phi(x)}{\beta} \right\} \alpha(dx)$$

where  $\phi$  may be any positive measurable function; in our case, it will represent the kernel function. With  $\phi(x) = v \mathbf{1}_A(x)$ , we get

$$\mathcal{L}(\phi) = -\log \mathbb{E} (\exp \{-v\Gamma(A)\}) = \int_A \log \left\{ 1 + \frac{v}{\beta} \right\} \alpha(dx) = \alpha(A) \log \left\{ 1 + \frac{v}{\beta} \right\},$$

i.e.,

$$\mathbb{E} (\exp \{-v\Gamma(A)\}) = \left( \frac{\beta}{v + \beta} \right)^{\alpha(A)}.$$

For bivariate analyses we choose  $\phi(x) = v_1 \mathbf{1}_{A_1}(x) + v_2 \mathbf{1}_{A_2}(x)$ , yielding

$$\begin{aligned}
\mathcal{L}(\phi) &= -\log \mathbb{E}(\exp\{-v_1\Gamma(A_1) - v_2\Gamma(A_2)\}) \\
&= -\log \mathbb{E}(\exp\{-v_1\Gamma(A_1 \setminus A_2) - (v_1 + v_2)\Gamma(A_1 \cap A_2) - v_2\Gamma(A_2 \setminus A_1)\}) \\
&= \int_{A_1 \setminus A_2} \log\left\{1 + \frac{v_1}{\beta}\right\} \alpha(dx) + \int_{A_1 \cap A_2} \log\left\{1 + \frac{v_1 + v_2}{\beta}\right\} \alpha(dx) \\
&\quad + \int_{A_2 \setminus A_1} \log\left\{1 + \frac{v_2}{\beta}\right\} \alpha(dx) \\
&= \alpha(A_1 \setminus A_2) \log\left\{1 + \frac{v_1}{\beta}\right\} + \alpha(A_1 \cap A_2) \log\left\{1 + \frac{v_1 + v_2}{\beta}\right\} + \alpha(A_2 \setminus A_1) \log\left\{1 + \frac{v_2}{\beta}\right\}
\end{aligned}$$

and therefore

$$\mathbb{E}(\exp\{-v_1\Gamma(A_1)\} - v_2\Gamma(A_2)\}) = \left(1 + \frac{v_1}{\beta}\right)^{-\alpha(A_1 \setminus A_2)} \left(1 + \frac{v_1 + v_2}{\beta}\right)^{-\alpha(A_1 \cap A_2)} \left(1 + \frac{v_2}{\beta}\right)^{-\alpha(A_2 \setminus A_1)}.$$

We propose to model  $\{\Lambda(x), x \in \mathcal{X}\}$  as a convolution using a 3D indicator kernel  $K(x, x')$  with an indicator set of finite volume used to convolute the gamma random field  $\Gamma(dx)$  (Wolpert and Ickstadt, 1998a), *i.e.*,  $\Lambda(x) = \int K(x, x')\Gamma(dx')$ . The shape of the kernel can be very general (although non indicator kernel usually do not lead to gamma marginal distributions), and particular choices may lead to non-stationary random fields, or to stationary random fields with given dependence properties such as full symmetry, separability or independence beyond some spatial distance or temporal lag. In order to limit model complexity and computational burden to a reasonable amount, we use the indicator kernel  $K(x, x') = \mathbf{1}_A(x - x')$ , for  $A \in \mathcal{B}_b(\mathcal{X})$ , where  $A$  is given as a slated elliptical cylinder, defining a  $d$ -dimensional set  $A_x$  that moves through  $\mathcal{X}$  according to some velocity vector. More precisely, let  $E(s, \gamma_1, \gamma_2, \phi)$  be an ellipse centered at  $s = (s_1, s_2) \in \mathbb{R}^2$  (see Figure 1-(a)) where its axes are rotated counterclockwise by the angle  $\phi$  with respect to the coordinate axes, and the semi-axes' lengths in the rotated coordinate system are  $\gamma_1$  and  $\gamma_2$ , respectively. A physical interpretation is that the ellipse describes the spatial influence zone of a storm centered at  $s$ . For the temporal dynamics, we assume that the ellipses (storms)  $E(s, \gamma_1, \gamma_2, \phi)$  move through space with a velocity  $\omega = (\omega_1, \omega_2) \in \mathbb{R}^2$  for a duration  $\delta > 0$ . The volume of the intersection of two slated elliptical cylinders (see Figure 1-(b)) is given by

$$V(s, t, s', t') = (\delta - |t - t'|)_+ \times \nu_2(E(s, \gamma_1, \gamma_2, \phi) \cap E(\tilde{s}, \gamma_1, \gamma_2, \phi))$$

where  $\tilde{s} = (\tilde{s}_1, \tilde{s}_2)$  with  $\tilde{s}_i = s'_i - |t' - t| \times \omega_i$ ,  $i = 1, 2$ .

For two fixed locations, the strength of dependence in the random field  $\Lambda(x)$  is an increasing monotone function of the intersection volume; other choices of  $A$  are possible, provided that we are able to calculate efficiently the volume of the intersection. To efficiently calculate the ellipse intersection area, we use an approach for finding the overlap area between two ellipses, which does not rely on proxy curves; see Hughes and Chraibi (2012)<sup>1</sup>.

In the sequel, we consider the measure  $\alpha(B) = \alpha\nu_d(B)/\nu_d(A)$  for  $B \in \mathcal{B}_b(\mathcal{X})$  where  $\nu_d(\cdot)$  is the Lebesgue measure on  $\mathbb{R}^d$ . It follows that  $\Lambda(x) \sim \text{Gamma}(\alpha, \beta)$ , as required for model (4). The univariate Laplace transform of  $\Lambda(x)$  is

$$LP_x^{(1)}(v) := \mathbb{E}(e^{-v\Lambda(x)}) = \left(\frac{\beta}{v + \beta}\right)^\alpha, \quad (8)$$

and the bivariate Laplace transform of  $\Lambda(x)$  and  $\Lambda(x')$  is

$$\begin{aligned} LP_{x,x'}^{(2)}(v_1, v_2) &:= \mathbb{E}(e^{-v_1\Lambda(x)-v_2\Lambda(x')}) \\ &= \left(\frac{\beta}{v_1 + \beta}\right)^{\alpha(A_x \setminus A_{x'})} \left(\frac{\beta}{v_1 + v_2 + \beta}\right)^{\alpha(A_x \cap A_{x'})} \left(\frac{\beta}{v_2 + \beta}\right)^{\alpha(A_{x'} \setminus A_x)}. \end{aligned} \quad (9)$$

### 3. JOINT TAIL BEHAVIOR OF THE HIERARCHICAL PROCESS

Extremal dependence in a bivariate random vector  $(Z_1, Z_2)$  can be explored based on the tail behavior of the conditional distribution  $\Pr(Z_1 > F_1^\leftarrow(q) | Z_2 > F_2^\leftarrow(q))$  as  $q$  tends to 1, where  $F_i^\leftarrow$ ,  $i = 1, 2$  denote the generalized inverse distribution functions of  $Z_i$  (Sibuya, 1960; Coles et al., 1999). The random vector  $(Z_1, Z_2)$  is said to be asymptotically dependent if a positive limit  $\chi$ , often referred to as the *tail correlation coefficient*, arises:

$$\chi(q) := \frac{\Pr(Z_1 > F_1^\leftarrow(q), Z_2 > F_2^\leftarrow(q))}{\Pr(Z_2 > F_2^\leftarrow(q))} \rightarrow \chi > 0, \quad q \rightarrow 1^-.$$

The case  $\chi = 0$  characterizes asymptotic independence.

To obtain a finer characterization of the joint tail decay rate under asymptotic independence, faster than the marginal tail decay rate, Coles et al. (1999) have introduced the  $\bar{\chi}$  index defined by through the

---

<sup>1</sup>The code is open source and can be downloaded from <http://github.com/chraibi/EEOver>

limit relation

$$\bar{\chi}(q) := \frac{2 \log \Pr(Z_2 > F_2^\leftarrow(q))}{\log \Pr(Z_1 > F_1^\leftarrow(q), Z_2 > F_2^\leftarrow(q))} - 1 \rightarrow \bar{\chi} \in (-1, 1], \quad q \rightarrow 1^-.$$

Larger values of  $|\bar{\chi}|$  correspond to stronger dependence. We now show that  $\{Z(x), x \in \mathcal{X}\}$  is an asymptotic independent process, *i.e.*, for all pairs  $(x, x') \in \mathcal{X}^2$  with  $x \neq x'$  the bivariate random vectors  $(Z(x), Z(x'))$  are asymptotically independent.

Owing to the stationarity of the process, it is easy to show that for any  $(x, x') \in \mathcal{X}^2$ ,  $x \neq x'$  and for values  $v$  exceeding a threshold  $u \geq 0$ , we get

$$\begin{aligned} \Pr(Z(x) > v) &= LP_x^{(1)}(v - u + \kappa) \\ &= \left(1 + \frac{v - u + \kappa}{\beta}\right)^{-\alpha(A_x)} \end{aligned}$$

and

$$\begin{aligned} \Pr(Z(x) > v, Z(x') > v) &= LP_{x,x'}^{(2)}(v - u + \kappa, v - u + \kappa) \\ &= \left(1 + \frac{v - u + \kappa}{\beta}\right)^{-\alpha(A_x \setminus A_{x'})} \left(1 + \frac{2v - 2u + 2\kappa}{\beta}\right)^{-\alpha(A_x \cap A_{x'})} \\ &\quad \times \left(1 + \frac{v - u + \kappa}{\beta}\right)^{-\alpha(A_{x'} \setminus A_x)}. \end{aligned}$$

To simplify notations, we set  $c_0 := \alpha(A_x)$ ,  $c_1 := \alpha(A_x \setminus A_{x'})$ ,  $c_2 := \alpha(A_x \cap A_{x'})$ ,  $c_3 := \alpha(A_{x'} \setminus A_x)$ , such that  $c_1 = c_3 = c_0 - c_2 \geq 0$  and  $c_1 + 2c_2 + c_3 = 2c_0$ . For  $c_2 = 0$  characterizing disjoint indicator sets  $A_x$  and  $A_{x'}$ , it is clear that  $Z(x)$  and  $Z(x')$  are independent. Now assume  $u = 0$  without loss of generality and  $x \neq x'$ ; then,

$$\begin{aligned} \chi_{x,x'}(v) &:= \frac{\Pr(Z(x) > v, Z(x') > v)}{\Pr(Z(x') > v)} \\ &= \left(1 + \frac{2v + 2\kappa}{\beta}\right)^{-c_2} \left(1 + \frac{v + \kappa}{\beta}\right)^{-c_1 - c_3 + c_0} \\ &= \left(1 + \frac{2v + 2\kappa}{\beta}\right)^{-c_2} \left(1 + \frac{v + \kappa}{\beta}\right)^{2c_2 - c_0} \\ &\sim 2^{-c_2} \left(\frac{v}{\beta}\right)^{c_2 - c_0}, \quad \text{for large } v. \end{aligned}$$

Since  $c_2 < c_0$ , we obtain

$$\chi_{x,x'} = 0.$$

We conclude that  $Z$  is an asymptotic independent process.

To characterize the faster joint tail decay, we calculate

$$\begin{aligned} \bar{\chi}_{xx'}(v) &:= \frac{2 \log \Pr(Z(x) > v)}{\log \Pr(Z(x) > v, Z(x') > v)} - 1 \\ &= \frac{-2c_0 \log (1 + (v + \kappa)/\beta)}{-c_1 \log(1 + (v + k)/\beta) - c_2 \log (1 + 2(v + k)/\beta) - c_3 \log(1 + (v + k)/\beta)} - 1 \\ &= \frac{2c_0}{c_1 + c_2 \frac{\log (1 + 2(v + k)/\beta)}{\log (1 + (v + k)/\beta)} + c_3} - 1. \end{aligned}$$

Taking the limit for  $v \rightarrow \infty$  yields

$$\bar{\chi}_{x,x'} = \frac{2c_0}{c_1 + c_2 + c_3} - 1 = \frac{c_2}{2c_0 - c_2},$$

which describes the ratio between the intersecting volume of  $A_x$  and  $A_{x'}$  and the volume of the union of these two sets. The value of  $\bar{\chi}$  confirms the asymptotic independence of the process  $Z$ . A larger intersecting volume between  $A_x$  and  $A_{x'}$  corresponds to stronger dependence.

#### 4. COMPOSITE LIKELIHOOD INFERENCE

To infer the tail behavior of the observed data process  $\{Z(x)\}$ , without loss of generality assumed to have generalized Pareto marginal distributions with shape parameter  $\alpha$ , we focus on values exceeding a fixed high threshold  $u$ . We let  $\theta$  denote the vector of unknown parameters. For simplicity, we assume that we have observed the excess values  $Y(s_i, t)$  for a factorial design of  $S$  locations  $s_i$ ,  $i = 1, \dots, S$  and  $T$  times  $t = 1, \dots, T$ .

By exploiting the tractability of intersecting volumes of two kernel sets, we focus on pairwise likelihood for efficient inference in our high-dimensional space-time set-up. The pairwise (weighted) log-likelihood

adds up the contributions  $f(Y(s_i, t), Y(s_j, t+k); \theta)$  of the censored observations  $Y(s_i, t), Y(s_j, t+k)$  and can be written

$$\text{pl}(\theta) = \sum_{t=1}^T \text{pl}_t(\theta) = \sum_{t=1}^T \sum_{k=0}^{\Delta_T} \sum_{i=1}^S \sum_{j=1}^S \{1 - \mathbb{1}\{i \geq j, k=0\}\} \log f(Y(s_i, t), Y(s_j, t+k); \theta) w_{s_i, s_j} \quad (10)$$

where  $w_{s_i, s_j}$  is a weight defined on  $[0, \infty)$ . We opt for a cut-off weight with  $w_{s_i, s_j} = 1$  if  $\|s_i - s_j\| \leq \Delta_S$  and 0 otherwise, which bypasses an explosion of the number of likelihood terms and shifts focus to relatively short-range distances where dependence matters most. This also avoids that the pairwise likelihood value (and therefore parameter estimation) is dominated by a large number of intermediate-range distances where dependence has already decayed to (almost) nil.

The contributions  $f(Y(x), Y(x'); \theta)$  are given by

$$f(y_1, y_2; \theta) = \begin{cases} \frac{\partial^2}{\partial v_1 \partial v_2} LP_{x, x'}^{(2)}(v_1, v_2) J(y_1) J(y_2) & y_1 > 0, y_2 > 0 \\ \left( -\frac{\partial}{\partial v_1} LP^{(1)}(v_1) + \frac{\partial}{\partial v_1} LP_{x, x'}^{(2)}(v_1, v_2) \right) J(y_1) & y_1 > 0, y_2 = 0 \\ \left( -\frac{\partial}{\partial v_2} LP^{(1)}(v_2) + \frac{\partial}{\partial v_2} LP_{x, x'}^{(2)}(v_1, v_2) \right) J(y_2) & y_1 = 0, y_2 > 0 \\ 1 - 2LP^{(1)}(v_1) + LP_{x, x'}^{(2)}(v_1, v_2) & y_1 = 0, y_2 = 0 \end{cases}$$

with  $v_i = (\kappa + 1) (1 + \xi^* y_i / \sigma^*)^{1/\xi^*} - 1$  and  $J(y_i) = \frac{\kappa+1}{\sigma^*} (1 + \frac{\xi^* y_i}{\sigma^*})^{1/\xi^* - 1}$ ,  $i = 1, 2$ . We provide analytical expressions for  $LP^{(1)}$  and  $LP_{x, x'}^{(2)}$  in the Appendix.

Under the assumption of temporal  $\alpha$ -mixing in the space-time random field  $\{\Lambda(x)\}$ , the maximum pairwise likelihood estimator  $\hat{\theta}$  is asymptotically normal for large  $T$ . The asymptotic variance is given by the inverse of the Godambe information matrix  $\mathcal{G}(\theta) = \mathcal{H}(\theta)[\mathcal{J}(\theta)]^{-1}\mathcal{H}(\theta)$ . Therefore, standard error evaluation requires consistent estimation of the matrices  $\mathcal{H}(\theta) = \mathbb{E}(-\nabla^2 \text{pl}(\theta))$  and  $\mathcal{J}(\theta) = \text{Var}(\nabla \text{pl}(\theta))$ . We estimate  $\mathcal{H}(\theta)$  with  $\hat{\mathcal{H}} = -\nabla^2 \text{pl}(\hat{\theta})$  and  $\mathcal{J}(\theta)$  through a subsampling technique (Carlstein, 1986), implemented as follows. We define  $B$  overlapping blocks  $D_b \subset \{1, \dots, T\}$ ,  $b = 1, \dots, B$ , containing  $d_b$  observations; we write  $\text{pl}_{D_b}$  for the pairwise likelihood (10) evaluated over the block  $D_b$ . The estimate of  $\mathcal{J}(\theta)$  is

$$\hat{\mathcal{J}} = \frac{T}{B} \sum_{b=1}^B \frac{1}{d_b} \nabla \text{pl}_{D_b}(\hat{\theta}) \nabla \text{pl}_{D_b}(\hat{\theta})'.$$

The estimates  $\hat{\mathcal{H}}$  and  $\hat{\mathcal{J}}$  allow us to calculate the composite likelihood information criterion (Varin and Vidoni, 2005)

$$\text{CLIC} = -2 \left[ \text{pl}(\hat{\theta}) - \text{tr}\{\hat{\mathcal{H}}^{-1}\hat{\mathcal{J}}\} \right]$$

with lower values of CLIC indicating a better fit.

## 5. SIMULATION STUDY

We assess the efficiency of the pairwise composite likelihood estimator through a small simulation study. We consider  $S = 15$  randomly chosen sites on  $[0, 1] \times [0, 1]$  (see Figure 2) observed at time points  $t = 1, \dots, T = 2000$ . The realizations of the gamma random field are simulated by adapting the algorithm of Wolpert and Ickstadt (1998b).

We fix parameters  $\xi = 1$ ,  $\sigma = 10$  and  $\kappa = 9$ , which fixes the exceedance probability to  $1 - p = 0.1$ . We design this simulation experiment with a view towards the subsequent real data analysis; therefore, we concentrate on estimating dependence parameters while treating the margins as known. For this reason, data is simulated according to a larger exceedance probability  $1 - p = 0.2$ , and we fix the site-dependent threshold  $u$  to the 90% sitewise empirical quantiles.

Two scenarios with different model complexity are considered, involving different specifications of the cylinder (see Table 1). Scenario A uses a circle-based cylinder without velocity while Scenario B comes with a slanted ellipse-based cylinder, yielding non null velocity. Technically, the model in Scenario A is over-parametrized since the rotation parameter  $\phi$  cannot change the volume of the cylinder.

Model parameters are estimated on 100 data replications using the composite likelihood approach developed in Section 4. We have considered a larger number of replications for some parameters combinations, but in general the number of 100 replications is enough to satisfactorily illustrate the estimation efficiency. The evaluation of  $\text{pl}(\theta)$  relies on the choice of  $\Delta_S$  and  $\Delta_T$ , where greater values increase the computational cost. Results in the literature indicate that using as much as possible or all pairs will not necessarily lead to an improvement in estimation owing to potential bias issues (see Huser and Davison (2014), for instance). We have considered different values of  $\Delta_T$  and have identified  $\Delta_T = 15$  as a good compromise for the estimation quality. The parameter  $\Delta_S$  has been set to 1 which is large enough with respect to the

spatial domain limits. Key results are illustrated in the boxplots in Figures 3 and 4.

When the cylinder is circle-based and without velocity (scenario A), boxplots in Figure 3 show that the parameters are overall well-estimated, even if the rotation parameter  $\phi$  is not identifiable. This implies robustness in the estimation since the presence of a potentially perturbing parameter does not affect the overall results.

In general, results are fairly good for the scenario B where the velocity is non null, but show some variability depending on the simulated parameters configuration. The estimates of the velocity present slightly higher variability, and the estimation of  $\omega_2$  appears slightly biased. On the other hand, the duration  $\delta$  and the lengths of the semi-axes of the ellipse ( $\gamma_1$  and  $\gamma_2$ ) are still well estimated. The angle  $\phi$  is identifiable in scenario B, but results are only a little better than with scenario A. We considered this as disappointing at first glance, but it may be due to the only moderate difference in the length of the semi-axes. To check this conjecture, we consider a modified scenario B where the second semi-axis is modified from  $\gamma_2 = 0.3$  to  $\gamma_2 = 0.5$  and other parameters remain unchanged. As illustrated by the boxplots in Figure 5, estimation of  $\phi$  clearly improves when the shape of the ellipse departs more strongly from a circular shape.

Despite a relatively small number of both spatial sites and time steps, this simulation study shows that the pairwise composite likelihood approach leads to reliable estimates of the model parameters that are well identifiable. We underline that results are consistently good whatever the complexity of the scenario.

## 6. REAL DATA EXAMPLE

### 6.1 Data

We apply our hierarchical model on precipitation extremes observed over a study region in the South of France. Extreme rainfall events usually occur during fall season. They are mainly due to southern winds driving warm and moist air from the Mediterranean sea towards the relatively cold mountainous areas of the Cevennes and the Alps, a situation which often provokes severe thunderstorms. The data was provided by Météo France (<https://publitheque.meteo.fr>). Our dataset is part of a query containing hourly observations at 208 rainfall stations for the years 1993 to 2014. To avoid modeling complex non stationary temporal patterns, we only keep the data from the September to January months, resulting in observations

over 80040 hours. We now consider 17 meteorological stations in a relative small region with elevations ranging from 140 to 1000 meters, whose observation series contain less than 10% of missing values over the study period. The spatial design of the stations is illustrated in Figure 6.

## 6.2 Exploratory analysis

We fit the univariate model (5) for each station by fixing a threshold  $u$  that corresponds to the empirical 99.5% quantile. We use such a rather high probability value since we have many observations, and there also is a substantial number of zero values such that a high quantile is needed to get into the tail region of the positive values. Figure 6 shows that clear spatial non stationarity arises in the marginal distributions.

Figure 7 displays empirical estimates of  $\chi(q)$  and  $\bar{\chi}(q)$  for probability values

$q = 0.95, 0.975, 0.99, 0.995, 0.999$  for the pairs  $Z(s, t), Z(s, t+h)$  with only temporal lag and pairs  $Z(s, t), Z(s', t)$  with only spatial lag. The curves in the bottom panels are the result of a smoothing procedure. These plots strongly support the assumption of asymptotic independence at all positive distances and at all positive temporal lags. Moreover, the strength of tail dependence as measured by the subasymptotic tail correlation value  $\chi(q)$  strongly decreases when considering exceedances over increasingly high thresholds, which provides another clear sign of continuously decreasing and ultimately vanishing dependence strength. On the other hand, the values of the sub-asymptotic dependence measure  $\bar{\chi}(q)$  (well adapted to asymptotic independence) decrease with increasing spatial distances or temporal lags, but they tend to stabilize at a non zero value. This behavior indicates the presence of residual tail dependence that vanishes only asymptotically.

## 6.3 Modeling spatio-temporal dependence

While the preceding exploratory analysis has shown that marginal distributions are not stationary, our model detailed in Section 2 requires a specific type of common marginal distributions. It would indeed be possible to extend the model to accommodate non stationary patterns (an example can be found in Bortot and Gaetan (2016)) and to jointly estimate marginal and dependence parameters. However, our focus here is to illustrate that our modeling strategy is capable to catch complex stationary spatio-temporal dependence patterns at large values, which would render joint estimation of margins and dependence highly

intricate. Therefore we fit a GP distribution separately to each site with thresholds chosen as the empirical 99.5% quantile. Next, we use the estimated parameters  $\hat{\xi}$  and  $\hat{\sigma}$  to transform the raw exceedances  $Y(x)$  observed at site  $x$  to exceedances  $\tilde{Y}(x)$  with cdf (5) such that  $\xi = 1$  and  $\sigma = \kappa + 1$ , *i.e.*,

$$\tilde{Y}(x) = (\kappa + 1) \left\{ \left( 1 + \frac{\hat{\xi} Y(x)}{\hat{\sigma}} \right)^{1/\hat{\xi}} - 1 \right\}.$$

Since  $\kappa$  satisfies the equality  $\Pr(\tilde{Y}(x) > 0) = (\kappa + 1)^{-1} = 0.005$ , see equation (6), we get  $\kappa = 199$ .

We fit our hierarchical models to the censored pretransformed data  $\tilde{Y}(x)$  by pairwise likelihood. We set the spatial cut-off value to  $\Delta_S = 43.011$ , which keeps around 60% of all distinct pairs of meteorological stations, and we choose the temporal cut-off lag as  $\Delta_T = 20$ . With these values, the exact number of pairs of observations is 296937420. The full pairwise likelihood would count around 925 *billion* pairs, which shows that we have attained a huge reduction. The pairwise likelihood has been coded in C; the optimization has been parallelized using the R library `parallel`. All calculations were carried out on a 2.300 GHz 32 core machine with 264GB of memory. Using 24 cores, one evaluation of the composite likelihood requires approximately 10 seconds. For calculating the standard errors and the CLIC, we use the previously described subsampling technique based on temporal windows, where we consider  $B = 1000$  overlapping blocks corresponding to 5000 hours, *i.e.*  $d_b = 17 \times 5000$ .

We have fitted our hierarchical model under two settings: with (M1) and without velocity (M1\*). Then, we have compared these two models to a simple but effective censored Gaussian space-time copula model (M2) (Bortot et al., 2000; Renard and Lang, 2007; Davison et al., 2013) in the class of asymptotically independent processes. Fitting model M2 corresponds to fit a censored Gaussian random field to transformed threshold exceedances; *i.e.*, we transform the original data to standard Gaussian marginal distributions  $G(x) = \Phi^\leftarrow(GP(\tilde{Y}(x)))$  (with  $\Phi$  the standard Gaussian cdf), and we suppose that  $\{G(x), x \in \mathcal{X}\}$  is a stationary standard Gaussian space-time random field. The space-time correlation function is chosen to be separable such that

$$\rho(x_1, x_2; \theta) = \exp(-h(s_1, s_2; \tau)/\psi_S) \exp(-|t_1 - t_2|/\psi_T) \quad (11)$$

with  $\theta = (\tau, \psi_S, \psi_T)$ . To remain coherent with the formulation of models M1 and M1\*, we assume an

anisotropic spatial correlation  $\rho(h(s_1, s_2; \tau); \psi_S)$  where  $h(s_1, s_2; \tau)$  denotes the scaled Mahalanobis distance

$$h(s_1, s_2; \tau) = \{(s_1 - s_2)' \Omega(\tau)^{-1} (s_1 - s_2)\}^{1/2}$$

with

$$\Omega(\tau) = \begin{pmatrix} \cos(\tau_1) & -\sin(\tau_1) \\ \sin(\tau_1) & \cos(\tau_1) \end{pmatrix} \begin{pmatrix} 1 & 0 \\ 0 & \tau_2^{-1} \end{pmatrix} \begin{pmatrix} \cos(\tau_1) & \sin(\tau_1) \\ -\sin(\tau_1) & \cos(\tau_1) \end{pmatrix}.$$

The Mahalanobis distance defines elliptical isocontours. Here,  $\tau_1$  is the angle with respect to the West-East direction, and  $\tau_2$  is the length ratio of the two principal axes. The model is isotropic for  $\tau_2 = 1$ .

Evaluation of the likelihood function of the model M2 necessitates performing inverse and determinant operations and numerical computation of multiple integrals (Genz and Bretz, 2009) both of which are computationally intractable for a large number of observations. Therefore we adopt again a pairwise likelihood approach.

Estimation results are summarized in Table 2. The CLIC in its last column shows a preference for our hierarchical models, with model M1 having the best value, followed closely by M1\*. When changing M1 to M1\*, the estimated duration changes only slightly. Estimates of  $\phi$  are different, but not surprisingly since the estimations of both semi-axis are very close. The estimates of  $\gamma_1$  and  $\gamma_2$  remain stable between M1\* and M1, which is also sign of the coherence of the two fitted models and gives strong support to considering estimated parameters values as reliable for physical interpretation.

To underpin the good fit of our models through visual diagnostics, Figure 8 shows estimated probabilities  $\Pr(Z(s, t) > q | Z(s', t') > q)$  along different directions and at different temporal lags  $|t - t'|$ . These plots suggest that the behavior of models M1 and M1\* is very close in practice; there is no strong preference for one model over the other.

Finally, we gain deeper insight into the joint tail structure of the fitted models by calculating empirical estimates  $\hat{p}_i(h)$  of the multivariate conditional probability

$$\chi_{s_i;h}^*(q) := \Pr(Z(s_j, t) > q, s_j \in \partial s_i | Z(s_i, t-h) > q)$$

where  $\partial s_i$  is the set of the four nearest neighbors of site  $s_i$ ,  $i = 1, \dots, 17$ . We compare these values with precise Monte-Carlo estimates  $\tilde{p}_i^{(j)}(h)$ ,  $j = 1, \dots, 200$ , based on a parametric bootstrap procedure with

200 simulations of the models  $M1$ ,  $M1^*$  and  $M2$ . We have then computed site specific root mean squared errors

$$\text{rmse}_i(h) = \left\{ \frac{\sum_{j=1}^{200} (\tilde{p}_i^{(j)}(h) - \hat{p}_i(h))^2}{200} \right\}^{1/2},$$

as well as the resulting total rmse,  $\text{rmse}(h) = \sum_{i=1}^{17} \text{rmse}_i(h)$ , as an overall measure of goodness of fit. Table 3 reports such values for fitted models using contemporaneous ( $h = 0$ ) or one lagged value ( $h = 1$ ), respectively. Our hierarchical models present the best fit in terms of rmse. While model  $M1^*$  performs slightly better for the threshold  $q_{0.995}$ , model  $M1$  seems to extrapolate better for larger values of the threshold such as  $q_{0.999}$ .

## 7. CONCLUSIONS

We have proposed a novel space-time model for threshold exceedances of data with asymptotically vanishing dependence strength. In the spirit of the hierarchical modeling paradigm with latent layers to capture complex dependence and time dynamics, it is based on a latent gamma convolution process with nonseparable space-time indicator kernels, and therefore amenable to physical interpretation. This framework leads to marginal and joint distributions that are available in closed form and are easy to handle in the extreme value context. More generally, a conditional independence assumption as in our model is convenient since it avoids handling tricky censoring schemes in high dimensions. In this respect, we can draw an interesting parallel to the max-stable Reich-Shaby process  $Z_{RS}(x)$  (Reich and Shaby, 2012), which is one of the more easily tractable spatial max-stable models and has a somewhat related construction; indeed, the inverted process  $1/Z_{RS}(x)$  can be represented as the embedding of a dependent latent process (based on  $\alpha$ -stable variables) for the rate of an exponential distribution.

We then have developed pairwise likelihood inference, which scales well with high-dimensional datasets and was shown to be reliable and efficient both statistically and computationally on complex parameter scenarios. We point out that handling observations over irregular time steps is possible with our model thanks to its definition over continuous time. While we think that MCMC-based Bayesian estimation of the relatively high number of parameters is out of reach principally due to the very high dimension of

the set of latent gamma variables in the model’s current formulation, we are confident that future efforts to tackle the conditional simulation of such space-time processes based on MCMC simulation with fixed parameters could be successful.

The application of our novel model to a high-dimensional real precipitation dataset from Southern France was motivated from clear evidence of asymptotic independence highlighted at an exploratory stage. It provides practical illustration of the high flexibility of our model and its capability to accurately predict extreme event probabilities for concomitant threshold exceedances in space and time. Based on meteorological knowledge about the precipitation processes in the study region, we had expected to estimate a clear velocity effect. As a matter of fact, the fitted velocity model appeared to be only slightly superior to other models in some aspects. This interesting finding may also be interpreted as evidence for the highly fragmented structure arising in precipitation processes at small spatial and temporal scales.

In ongoing work, we aim to adapt the current latent process construction to the multivariate set-up by considering constructions with common factors, hierarchical structures and extensions to asymptotic dependence. Ultimately, we expect these novelties to open perspectives towards multivariate space-time modeling with scenarios of partial or full asymptotic dependence.

#### ACKNOWLEDGMENT

This work was supported by the French national programme LEFE/INSU. The authors are grateful to Julie Carreau (IRD HydroSciences, Montpellier, France) for helping them in collecting the data from the Meteo France database.

## APPENDIX : ANALYTICAL EXPRESSIONS FOR THE PAIRWISE LIKELIHOOD

Let  $LP^{(1)}(v)$  and  $LP_{x,x'}^{(2)}(v_1, v_2)$ ,  $x \neq x'$  be the univariate and bivariate Laplace transform of  $\Lambda(A_x)$  i.e.

$$LP^{(1)}(v) := \mathbb{E} (e^{-v\Lambda(A_x)}) = \left( \frac{\beta}{v + \beta} \right)^{c_0},$$

and

$$LP_{x,x'}^{(2)}(v_1, v_2) := \mathbb{E} (e^{-v_1\Lambda(A_x) - v_2\Lambda(A_{x'})}) = \left( \frac{\beta}{v_1 + \beta} \right)^{c_1} \left( \frac{\beta}{v_1 + v_2 + \beta} \right)^{c_2} \left( \frac{\beta}{v_2 + \beta} \right)^{c_3}$$

with  $c_0 = \alpha(A_x)$ ,  $c_1 = \alpha(A_x \setminus A_{x'})$ ,  $c_2 = \alpha(A_x \cap A_{x'})$ ,  $c_3 = \alpha(A_{x'} \setminus A_x)$ .

We have

$$\begin{aligned} \frac{\partial}{\partial v} LP^{(1)}(v) &= -c_0 \beta^{c_0} (v + \beta)^{-c_0-1} \\ \frac{\partial}{\partial v_1} LP_{x,x'}^{(2)}(v_1, v_2) &= -\beta^{c_1+c_2+c_3} \left\{ c_1 (v_1 + \beta)^{-c_1-1} (v_1 + v_2 + \beta)^{-c_2} (v_2 + \beta)^{-c_3} \right. \\ &\quad \left. + c_2 (v_1 + \beta)^{-c_1} (v_1 + v_2 + \beta)^{-c_2-1} (v_2 + \beta)^{-c_3} \right\} \\ \frac{\partial}{\partial v_2} LP_{x,x'}^{(2)}(v_1, v_2) &= -\beta^{c_1+c_2+c_3} \left\{ c_3 (v_1 + \beta)^{-c_1} (v_1 + v_2 + \beta)^{-c_2} (v_2 + \beta)^{-c_3-1} \right. \\ &\quad \left. + c_2 (v_1 + \beta)^{-c_1} (v_1 + v_2 + \beta)^{-c_2-1} (v_2 + \beta)^{-c_3} \right\} \\ \frac{\partial}{\partial v_1 \partial v_2} LP_{x,x'}^{(2)}(v_1, v_2) &= \beta^{c_1+c_2+c_3} \left\{ c_1 c_2 (v_1 + \beta)^{-c_1-1} (v_1 + v_2 + \beta)^{-c_2-1} (v_2 + \beta)^{-c_3} \right. \\ &\quad \left. + c_1 c_3 (v_1 + \beta)^{-c_1-1} (v_1 + v_2 + \beta)^{-c_2} (v_2 + \beta)^{-c_3-1} \right. \\ &\quad \left. + c_2 (c_2 + 1) (v_1 + \beta)^{-c_1} (v_1 + v_2 + \beta)^{-c_2-2} (v_2 + \beta)^{-c_3} \right. \\ &\quad \left. + c_2 c_3 (v_1 + \beta)^{-c_1} (v_1 + v_2 + \beta)^{-c_2-1} (v_2 + \beta)^{-c_3-1} \right\} \end{aligned}$$

## References

Bacro, J. N., Gaetan, C., and Toulemonde, G. (2016), “A flexible dependence model for spatial extremes,” *Journal of Statistical Planning and Inference*, 172, 36–52.

Barndorff-Nielsen, O. E., Lunde, A., Shepard, N., and Veraat, A. E. D. (2014), “Integer-valued Trawl Processes: A Class of Stationary Infinitively Divisible Processes,” *Scandinavian Journal of Statistics*, 41, 693–724.

Bortot, P., Coles, S., and Tawn, J. (2000), “The multivariate Gaussian tail model: an application to oceanographic data,” *Journal of the Royal Statistical Society: Series C (Applied Statistics)*, 49, 31–49.

Bortot, P., and Gaetan, C. (2014), “A latent process model for temporal extremes,” *Scandinavian Journal of Statistics*, 41, 606–621.

Bortot, P., and Gaetan, C. (2016), “Latent Process Modelling of Threshold Exceedances in Hourly Rainfall Series,” *Journal of Agricultural, Biological, and Environmental Statistics*, 21, 531–547.

Carlstein, A. (1986), “The use of subseries values for estimating the variance of a general statistic from a stationary sequence,” *The Annals of Statistics*, 14, 1171–1179.

Casson, E., and Coles, S. G. (1999), “Spatial regression models for extremes,” *Extremes*, 1, 449–468.

Coles, S., Heffernan, J., and Tawn, J. (1999), “Dependence measures for extreme value analyses,” *Extremes*, 2, 339–365.

Cooley, D., Nychka, D., and Naveau, P. (2007), “Bayesian Spatial Modeling of Extreme Precipitation Return Levels,” *Journal of the American Statistical Association*, 102, 824–840.

Davis, R. A., Klüppelberg, C., and Steinkohl, C. (2013a), “Max-stable processes for modeling extremes observed in space and time,” *Journal of the Korean Statistical Society*, 42, 399–414.

Davis, R. A., Klüppelberg, C., and Steinkohl, C. (2013b), “Statistical inference for max-stable processes in space and time,” *Journal of the Royal Statistical Society*, 75, 791–819.

Davis, R. A., and Mikosch, T. (2008), “Extreme value theory for space-time processes with heavy-tailed distributions,” *Stochastic Processes and their Applications*, 118, 560–584.

Davison, A. C., and Gholamrezaee, M. M. (2012), “Geostatistics of extremes,” *Proceedings of the Royal Society London, Series A*, 468, 581–608.

Davison, A. C., Huser, R., and Thibaud, E. (2013), “Geostatistics of dependent and asymptotically independent extremes,” *Journal of Mathematical Geosciences*, 45, 511–529.

Davison, A. C., Padoan, S. A., and Ribatet, M. (2012), “Statistical modelling of spatial extremes,” *Statistical Science*, 27, 161–186.

de Haan, L., and Ferreira, A. (2006), *Extreme Value Theory: an Introduction*, New-York: Springer.

Ferguson, T. S. (1973), “A Bayesian Analysis of Some Nonparametric Problems,” *The Annals of Statistics*, 1, 209–230.

Ferreira, A., and de Haan, L. (2014), “The generalized Pareto process; with a view towards application and simulation,” *Bernoulli*, 20, 1717–1737.

Gaetan, C., and Grigoletto, M. (2007), “A hierarchical model for the analysis of spatial rainfall extremes,” *Journal of Agricultural Biological and Environmental Statistics*, 12, 434–449.

Genz, A., and Bretz, F. (2009), *Computation of Multivariate Normal and t Probabilities*, New York, NY: Springer.

Hughes, G. B., and Chraibi, M. (2012), “Calculating ellipse overlap areas,” *Computing and Visualization in Science*, 15, 291–301.

Huser, R., and Davison, A. C. (2014), “Space-time modelling of extreme events,” *Journal of the Royal Statistical Society: Series B*, 76, 439–461.

Huser, R., Opitz, T., and Thibaud, E. (2017), “Bridging Asymptotic Independence and Dependence in Spatial Extremes Using Gaussian Scale Mixtures,” *Spatial Statistics*, To appear.

Joe, H. (1997), *Multivariate Models and Dependence Concepts*, London: Chapman & Hall.

Kabluchko, Z., Schlather, M., and de Haan, L. (2009), “Stationary max-stable fields associated to negative definite functions,” *The Annals of Probability*, 37, 2042–2065.

Morris, S. A., Reich, B. J., Thibaud, E., and Cooley, D. (2017), “A space-time skew-t model for threshold exceedances,” *Biometrics*, To appear.

Nieto-Barajas, L. E., and Huerta, G. (2017), “Spatio-temporal pareto modelling of heavy-tail data,” *Spatial Statistics*, 20, 92–109.

Opitz, T. (2013), “Extremal t processes: elliptical domain of attraction and a spectral representation,” *Journal of Multivariate Analysis*, 122, 409–413.

Opitz, T. (2016), “Modeling asymptotically independent spatial extremes based on Laplace random fields,” *Spatial Statistics*, 16, 1–18.

Reich, B. J., and Shaby, B. A. (2012), “A hierarchical max-stable spatial model for extreme precipitation,” *The Annals of Applied Statistics*, 6(4), 1430–1451.

Reiss, R., and Thomas, M. (2007), *Statistical Analysis of Extreme Values*, third edn, Basel: Birkhäuser.

Renard, B., and Lang, M. (2007), “Use of a Gaussian copula for multivariate extreme value analysis: Some case studies in hydrology,” *Advances in Water Resources*, 30, 897 – 912.

Sang, H., and Gelfand, A. (2009), “Hierarchical modeling for extreme values observed over space and time,” *Environmental and Ecological Statistics*, 16, 407–426.

Schlather, M. (2002), “Models for stationary max-stable random fields,” *Extremes*, 5, 33–44.

Sibuya, M. (1960), “Bivariate extreme statistics,” *Annals of the Institute of Statistical Mathematics*, 11, 195–210.

Smith, R. L. (1990), “Max-stable processes and spatial extremes,” *Preprint*, University of Surrey.

Thibaud, E., Mutzner, R., and Davison, A. C. (2013), “Threshold modeling of extreme spatial rainfall,” *Water Resources Research*, 49, 4633–4644.

Thibaud, E., and Opitz, T. (2015), “Efficient inference and simulation for elliptical Pareto processes,” *Biometrika*, 102(4), 855–870.

Varin, C., and Vidoni, P. (2005), “A note on composite likelihood inference and model selection,” *Biometrika*, 52, 519–528.

Wadsworth, J., and Tawn, J. (2012), “Dependence modelling for spatial extremes,” *Biometrika*, 99, 253–272.

Wolpert, R. L., and Ickstadt, K. (1998a), “Poisson/Gamma random fields for spatial statistics,” *Biometrika*, 85, 251–267.

Wolpert, R. L., and Ickstadt, K. (1998b), “Simulation of Lévy Random Fields,” in *Practical Nonparametric and Semiparametric Bayesian Statistics*, eds. D. Dey, P. Müller, and D. Sinha, New York, NY: Springer New York, pp. 227–242.

Parameters						
Scenario	$\gamma_1$	$\gamma_2$	$\phi$	$\delta$	$\omega_1$	$\omega_2$
A	0.2	0.2	-	10	0.00	0.00
B	0.2	0.3	$\pi/4$	5	0.05	0.10

Table 1: Design of the two simulation scenarios.

Model	Parameters						
M1	$\gamma_1$	$\gamma_2$	$\phi$	$\delta$	$\omega_1$	$\omega_2$	CLIC
	1.414E+02	1.250E+02	1.266E+00	1.960E+01	1.266E-04	-8.047E-01	36 980 402
	(5.539E-03)	(6.537E-03)	(1.373E-01)	(3.803E-01)	(5.773E-05)	(1.860E-01)	
M1*	$\gamma_1$	$\gamma_2$	$\phi$	$\delta$	$\omega_1$	$\omega_2$	CLIC
	1.281E+02	1.538E+02	3.126E-05	1.885E+01	0	0	36 980 728
	(1.091E-02)	(9.681E-03)	(2.350E-07)	(5.011E-01)	-	-	
M2	$\psi_S$	$\psi_T$	$\tau_1$	$\tau_2$			CLIC
	1.086E+02	8.253E+00	1.470E-01	1.466E+00			36 985 103
	(4.288E+00)	(2.430E-01)	(9.335E-02)	(9.254E-02)			

Table 2: Estimates and CLIC values of fitted models. Standard errors are reported in parentheses.

	rmse(0)		rmse(1)	
	$q_{0.995}$	$q_{0.999}$	$q_{0.995}$	$q_{0.999}$
M1	0.823	0.821	0.431	0.637
M1*	0.747	0.885	0.417	0.677
M2	1.557	2.127	1.301	1.270

Table 3: Total root mean squared errors for the estimates of  $\chi_{s_i;h}^*(q)$ .

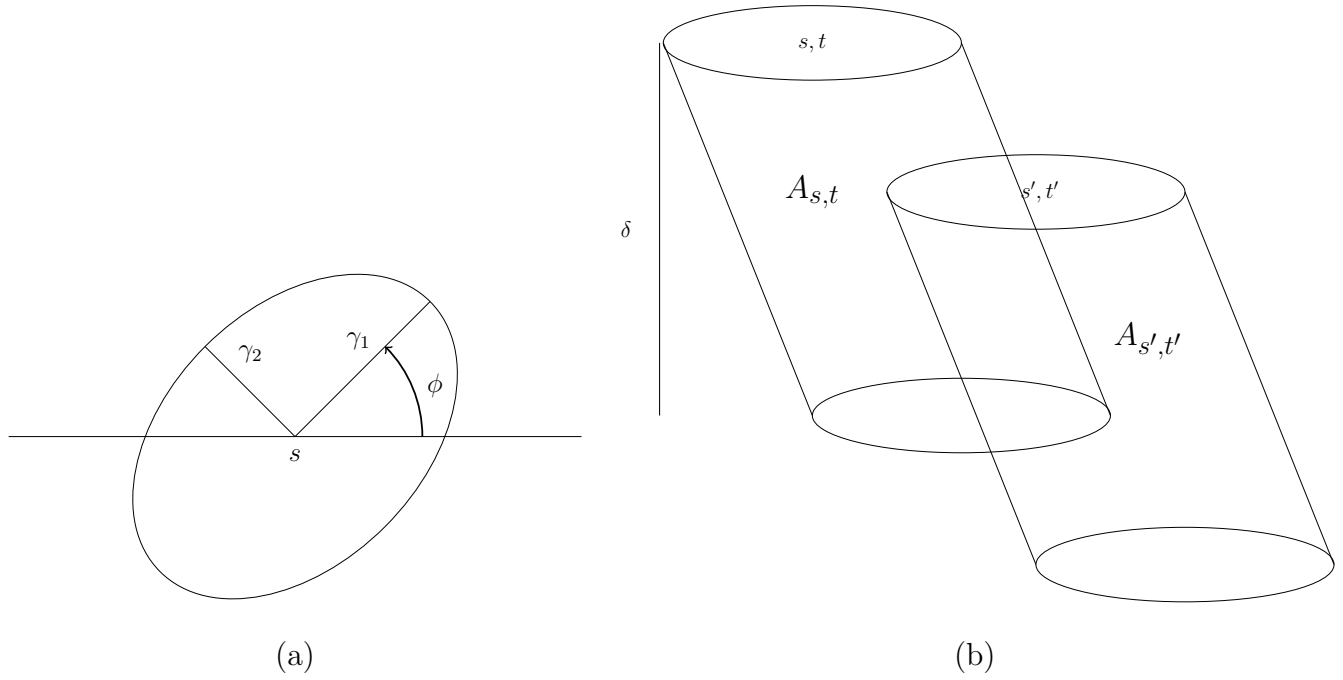


Figure 1: On the left: the ellipse  $E(s, \gamma_1, \gamma_2, \phi)$  centered at  $s$ ; on the right: the intersection of two slated elliptical cylinders  $A_{s,t}$  and  $A_{s',t'}$  with duration  $\delta$ .

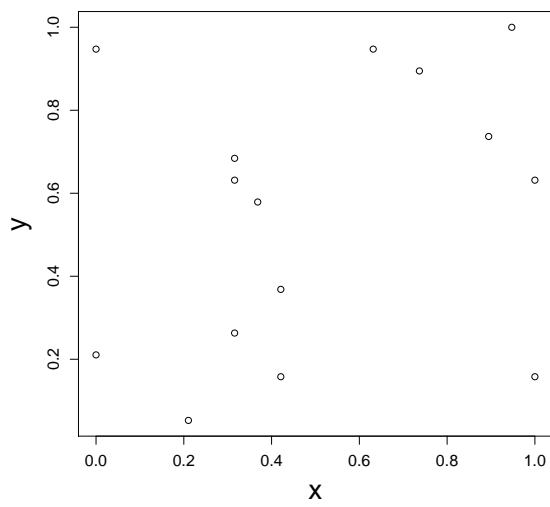


Figure 2: The spatial configuration of sites used for the simulation study.

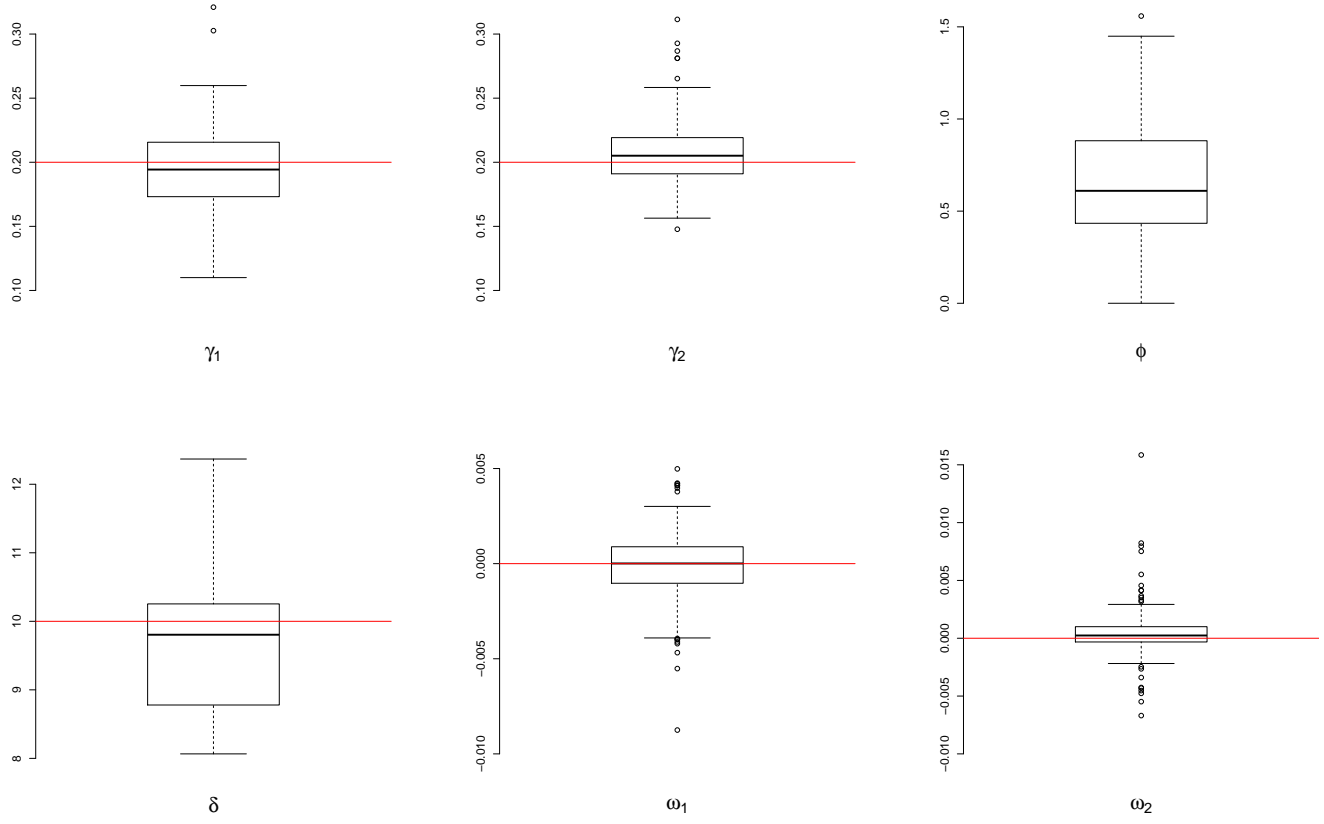


Figure 3: Scenario A: boxplots of parameters estimates from 100 simulated datasets.

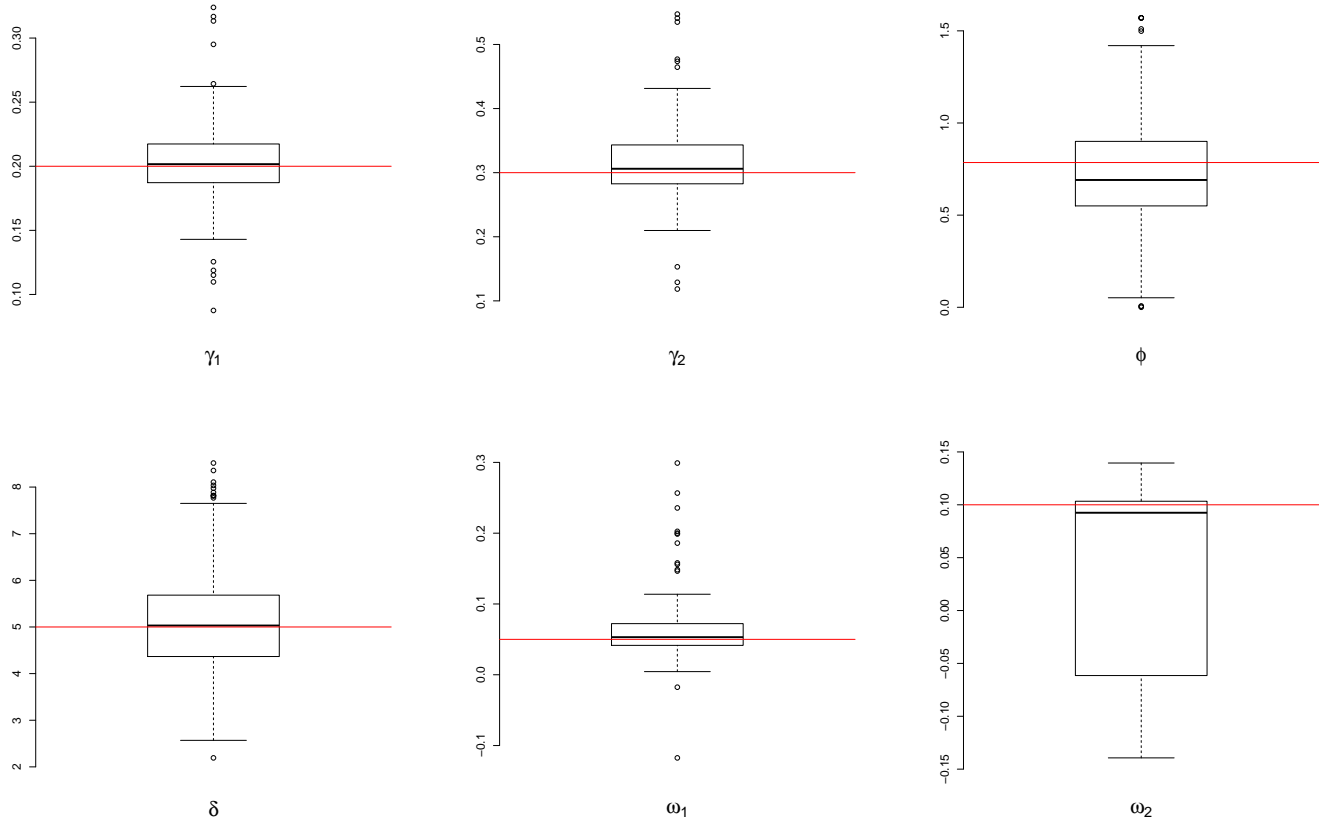


Figure 4: Scenario B: boxplots of parameters estimates from 100 simulated datasets.

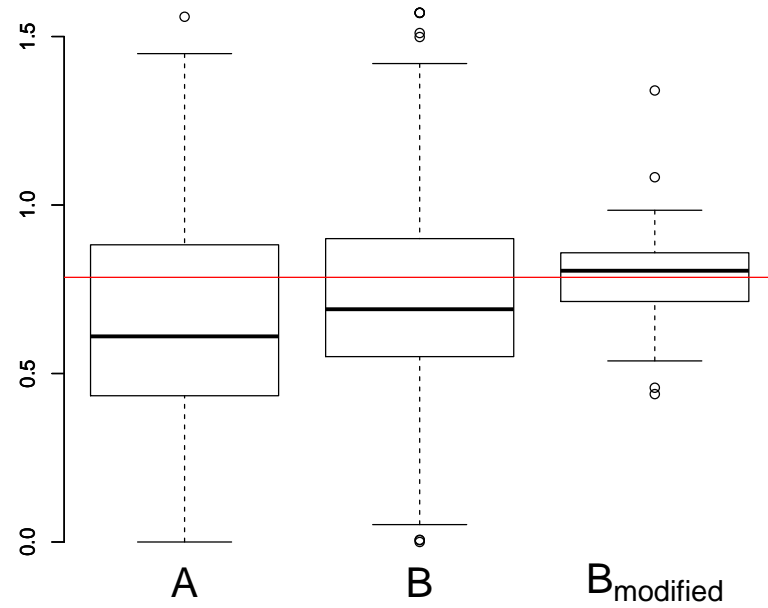


Figure 5: Boxplots of  $\phi$  estimations according to scenario A, scenario B and a modified scenario B with  $\gamma_2 = 0.5$ .

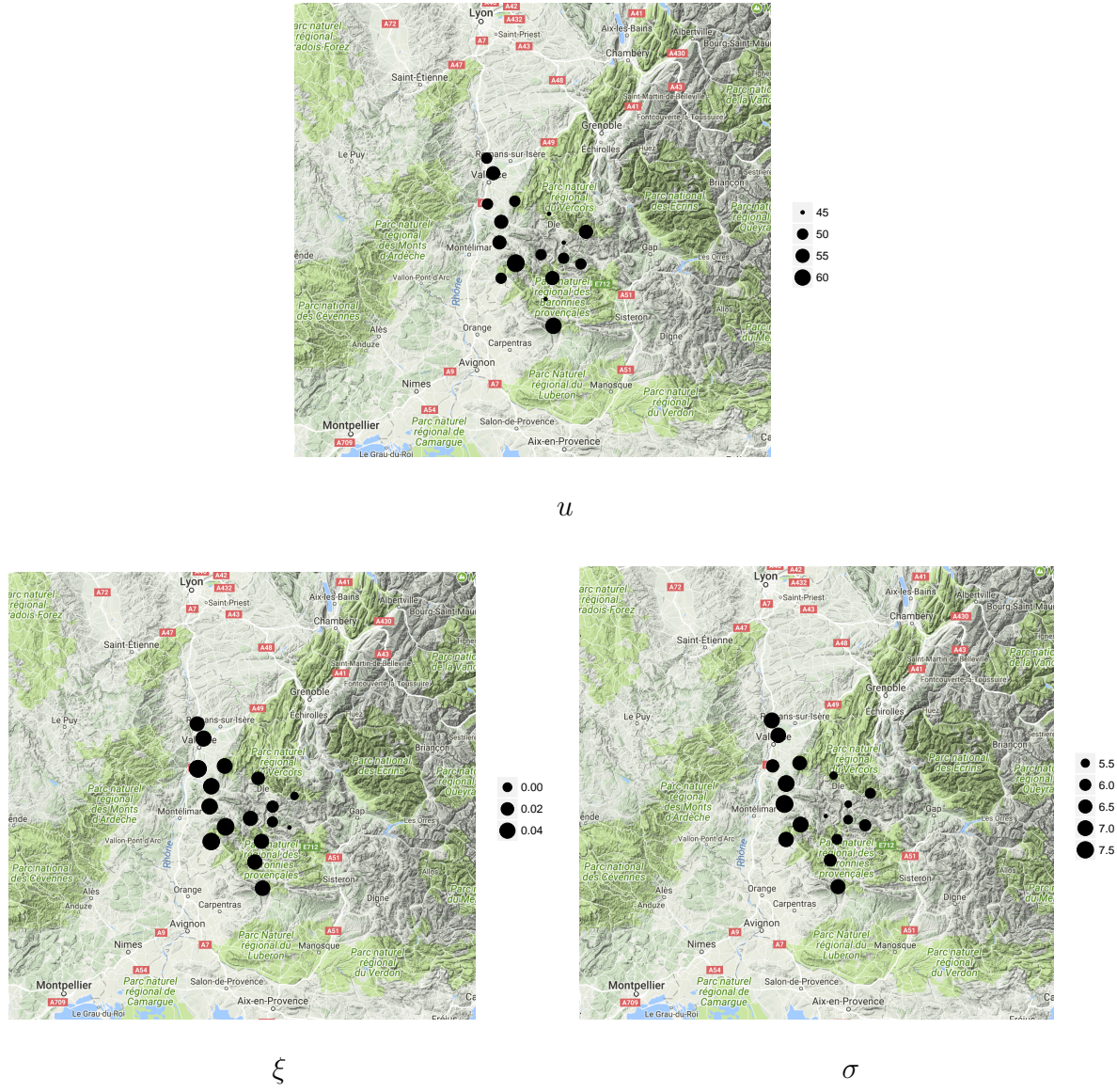


Figure 6: Topographic map of the region in Southern France showing the meteorological stations selected for our study. Dots correspond to the stations used for fitting; their diameter is proportional to empirical 99.5% quantiles  $u(s)$  (upper plot) and to estimates of the GPD parameters  $\xi$  (lower left plot) and  $\sigma$  (lower right plot).

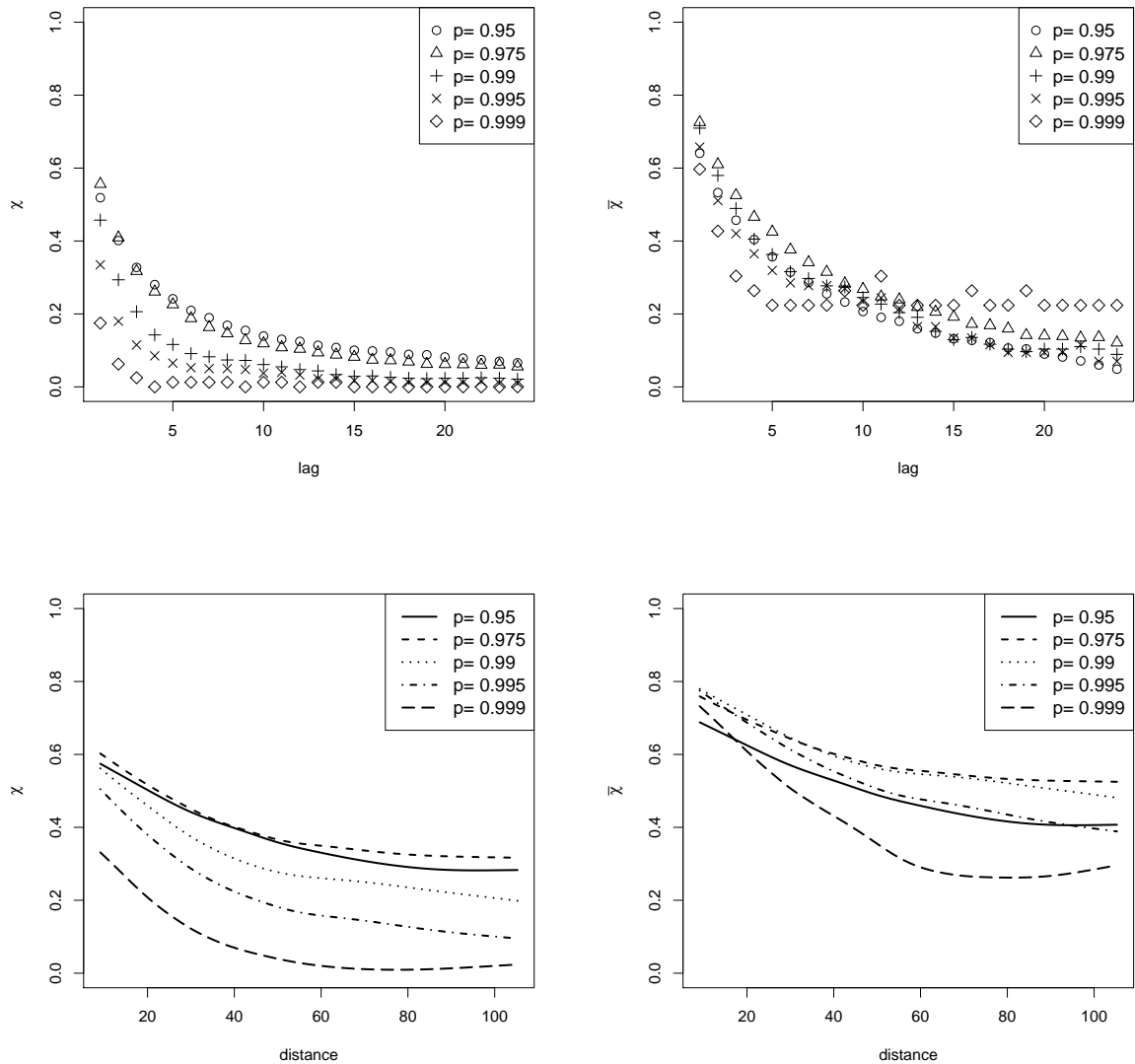


Figure 7: Empirical estimates of  $\chi(q)$  (left panels) and  $\bar{\chi}(q)$  (right panels) coefficients.

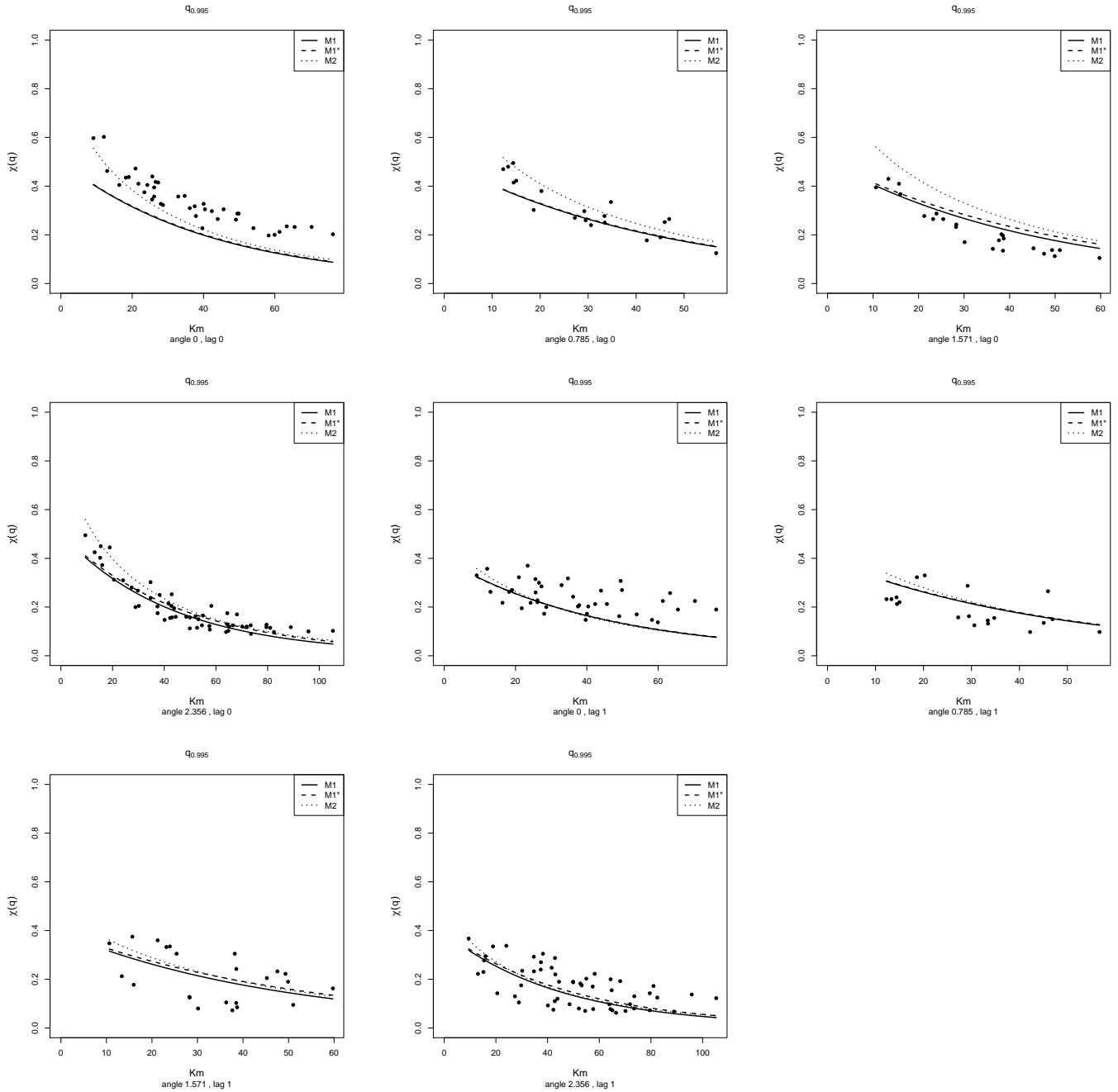


Figure 8: Estimated probabilities  $\Pr(Z(s,t) > q | Z(s',t') > q)$  along different directions (expressed in radians) and at different temporal lags. Dotted points correspond to empirical estimates. The value  $q$  is fixed to the empirical 99.5% quantile.